HHS Public Access

Author manuscript

Neuroimage. Author manuscript; available in PMC 2024 February 15.

Published in final edited form as:

Neuroimage. 2024 February 01; 286: 120509. doi:10.1016/j.neuroimage.2024.120509.

Direct comparison between ^{18}F-Flortaucipir tau PET and quantitative susceptibility mapping in progressive supranuclear palsy

Ryota Satoh[a], **Farwa Ali**[a], **Hugo Botha**[a], **Val J. Lowe**[b], **Keith A. Josephs**[a], **Jennifer L. Whitwell**[b,*]

[a]Department of Neurology, Mayo Clinic, Rochester, MN, USA

[b]Department of Radiology, Mayo Clinic, 200 1st St SW, 55905, Rochester, MN, USA

Abstract

Purpose: The pattern of flortaucipir tau PET uptake is topographically similar to the pattern of magnetic susceptibility in progressive supranuclear palsy (PSP); both with increased signal in subcortical structures such as the basal ganglia and midbrain, suggesting that they may be closely related. However, their relationship remains unknown since no studies have directly compared these two modalities in the same PSP cohort. We hypothesized that some flortaucipir uptake in PSP is associated with magnetic susceptibility, and hence iron deposition. The aim of this study was to evaluate the regional relationship between flortaucipir uptake and magnetic susceptibility and to examine the effects of susceptibility on flortaucipir uptake in PSP.

Methods: Fifty PSP patients and 67 cognitively normal controls were prospectively recruited and underwent three Tesla MRI and flortaucipir tau PET scans. Quantitative susceptibility maps were reconstructed from multi-echo gradient-echo MRI images. Region of interest (ROI) analysis was performed to obtain flortaucipir and susceptibility values in the subcortical regions. Relationships between flortaucipir and susceptibility signals were evaluated using partial correlation analysis in the subcortical ROIs and voxel-based analysis in the whole brain. The effects of susceptibility on flortaucipir uptake were examined by using the framework of mediation analysis.

*Corresponding author: whitwell.jennifer@mayo.edu (J.L. Whitwell).

Declaration of competing interest

VJL serves as consultant for Bayer Schering Pharma, Philips Molecular Imaging, Piramal Imaging, AVID Radiopharmaceuticals, Eisai Inc., Eli Lilly, and GE Healthcare and receives research support from GE Healthcare, Siemens Molecular Imaging, AVID Radiopharmaceuticals, the NIH (NIA, NCI), and the MN Partnership for Biotechnology and Medical Genomics. No other potential conflict of interest relevant to this article was reported.

Supplementary materials

Supplementary material associated with this article can be found, in the online version, at doi:10.1016/j.neuroimage.2024.120509.

CRediT authorship contribution statement

Ryota Satoh: Formal analysis, Investigation, Methodology, Software, Writing – original draft. **Farwa Ali:** Resources, Writing – review & editing. **Hugo Botha:** Resources, Writing – review & editing. **Val J. Lowe:** Methodology, Resources, Writing – review & editing. **Keith A. Josephs:** Conceptualization, Funding acquisition, Methodology, Project administration, Resources, Supervision, Writing – review & editing. **Jennifer L. Whitwell:** Conceptualization, Funding acquisition, Methodology, Project administration, Supervision, Writing – review & editing.

Results: Both flortaucipir and susceptibility were greater in PSP compared to controls in the putamen, pallidum, subthalamic nucleus, red nucleus, and cerebellar dentate ($p<0.05$). The ROI-based and voxel-based analyses showed that these two signals were positively correlated in these five regions ($r = 0.36–0.59$, $p<0.05$). Mediation analysis showed that greater flortaucipir uptake was partially explained by susceptibility in the putamen, pallidum, subthalamic nucleus, and red nucleus, and fully explained in the cerebellar dentate.

Conclusions: These results suggest that some of the flortaucipir uptake in subcortical regions in PSP is related to iron deposition. These findings will contribute to our understanding of the mechanisms underlying flortaucipir tau PET findings in PSP and other neurodegenerative diseases.

Keywords

Flortaucipir; Tau PET; Iron; Quantitative susceptibility mapping; PSP

1. Introduction

Flortaucipir was the first tau PET tracer to receive FDA approval for the assessment of tau deposition in Alzheimer's disease (AD) (Mattay et al., 2020). This tracer was originally developed and optimized for the assessment of AD tau, but it has also been widely used to study other tauopathies such as progressive supranuclear palsy (PSP) (Jin et al., 2023). PSP is one of the 4 repeat (4R) tauopathies characterized by oculomotor dysfunction, postural instability, akinesia, and cognitive dysfunction (Hauw et al., 1994; Hoglinger et al., 2017). Many PSP studies have found abnormal flortaucipir uptake in subcortical structures such as the basal ganglia and midbrain (Cho et al., 2017; Passamonti et al., 2017; Smith et al., 2017; Whitwell et al., 2017b), which is generally consistent with the expected distribution of PSP tau pathology (Kovacs et al., 2020; Williams et al., 2007). Some studies also showed that flortaucipir PET successfully differentiated PSP from AD (Passamonti et al., 2017; Whitwell et al., 2017b) and Parkinson's disease (Cho et al., 2017), suggesting that it could be a supportive biomarker for PSP (Whitwell et al., 2017a).

However, it is not yet fully understood whether the flortaucipir uptake in each subcortical region truly reflects 4R tau or falsely binds to other off-target compounds. This is because many postmortem studies have consistently shown little to no binding of flortaucipir to 4R tau in PSP (Lowe et al., 2016; Marquie et al., 2017). In addition, the subcortical structures largely coincide with regions of abundant iron and monoamine oxidase, which may cause off-target binding of flortaucipir (Lowe et al., 2016; Vermeiren et al., 2018). Indeed, a few studies have shown that flortaucipir signals and iron-related MRI signals in the basal ganglia are positively associated in cognitively normal subjects and AD patients (Choi et al., 2018; Cogswell et al., 2021), although to our knowledge, similar papers are not available for PSP (Cogswell and Fan, 2023). Further studies are needed to better understand the underlying mechanisms of subcortical flortaucipir uptake in PSP.

Quantitative susceptibility mapping (QSM) is an advanced MRI technique that estimates the distribution of magnetic susceptibility in vivo (Wang and Liu, 2015). QSM is strongly associated with iron concentration in subcortical regions (Langkammer et al., 2012), and therefore many studies have utilized QSM to evaluate abnormal iron deposition in PSP

(Ito et al., 2017; Sjostrom et al., 2017, 2019). Patterns of increased magnetic susceptibility appear to be topographically similar to patterns of flortaucipir uptake in PSP; both are increased in subcortical areas such as the basal ganglia, midbrain, and cerebellar dentate, suggesting that these two signals are closely related. However, to our knowledge, no studies have directly compared these two modalities in the same PSP cohort.

To better understand the underlying mechanisms of subcortical flortaucipir uptake, we directly compared flortaucipir PET and QSM in the same PSP cohort and then examined the effects of susceptibility on flortaucipir uptake in PSP. We hypothesized that some subcortical flortaucipir uptake is associated with increased magnetic susceptibility in PSP.

2. Methods

2.1. Participants

Fifty-three patients diagnosed with PSP based on consensus criteria (Hoglinger et al., 2017) were prospectively recruited from May 2018 to February 2023 by the Neurodegenerative Research Group (NRG), Mayo Clinic, Rochester, Minnesota. All patients underwent detailed neurological tests including the Montreal Cognitive Assessment (MoCA) (Nasreddine et al., 2005), the Movement Disorders Society sponsored revision of the Unified Parkinson's Disease Rating Scale part III (MDS-UPDRS III) (Goetz et al., 2008), the PSP rating scale (Golbe and Ohman-Strickland, 2007), and the PSP Saccadic Impairment Scale (PSIS) (Whitwell et al., 2011), as well as an ^{18}F-flortaucipir PET scan and a 3 Tesla MRI scan with a multi-echo gradient echo sequence. Magnetic Resonance Parkinsonism Index (MRPI) (Quattrone et al., 2008) was measured from 3D T1-weighted MR images using ITK-SNAP software as previously described (Grijalva et al., 2022). Three patients were excluded because they had intracranial hemorrhages on QSM images, leaving 50 PSP patients. All 50 patients were given a PSP syndromic diagnosis according to the MDS-PSP diagnostic criteria (Grimm et al., 2019; Hoglinger et al., 2017), as previously described in detail (Grijalva et al., 2022). Of the 50 PSP patients, 19 were diagnosed with PSP-Richardson syndrome, ten with PSP-Parkinsonism, seven with PSP-progressive gait freezing, five with PSP-postural instability, four with PSP-corticobasal syndrome, two with PSP-speech/language, and one with PSP-frontal (Hoglinger et al., 2017). A further two patients had clinical features of PSP plus prominent upper motor neuron signs such as spasticity, hyperreflexia, clonus and Babinski sign (Grijalva et al., 2022; Josephs et al., 2006) and were diagnosed with PSP-corticospinal. Sixty-seven cognitively normal subjects who did not have any complaints of cognitive, motor, or behavioral abnormalities and had a score of ≥23 on the MoCA test (Carson et al., 2018) and 0 on the Hoehn and Yahr (Hoehn and Yahr, 1967) were also recruited by NRG over the same time period, and underwent flortaucipir PET and MRI scans with the same protocols. We included all recruited cognitively normal subjects to provide the most power to evaluate relationships between flortaucipir and susceptibility. This study was approved by the Mayo Clinic Institutional Review Board (IRB#: 15-004618), and informed consent was obtained from all participants.

2.2. MRI and PET analysis

All patients underwent a standardized MRI protocol on a 3.0 Tesla scanner (Magnetom Prisma, Siemens Healthineers), including a 3D magnetization prepared rapid acquisition gradient echo (MPRAGE) sequence and a 3D multi-echo gradient echo sequence, as described in previous papers (Satoh et al., 2023a; Singh et al., 2022). The scan parameters of the gradient echo sequence were repetition time of 28.0 ms, echo times of 6.7 ms, 10.6 ms, 14.5 ms, 18.4 ms, and 22.4 ms, flip angle of 15°, 20 cm field of view, in-plane acquisition matrix of 384×269, slice number of 88, slice thickness of 1.8 mm, and parallel imaging acceleration factor of 2.0.

The MRI and following PET images were processed on the high-performance computing environment (mForge) hosted by the National Center for Supercomputing Applications using NRG in-house developed pipelines (RS). The T1-weighted images from the MPRAGE scan were segmented into gray and white matter using templates and settings from the Mayo Clinic Adult Lifespan Template (MCALT: https://www.nitrc.org/projects/mcalt/). Brain atlases for subcortical regions of interests (ROIs) were nonlinearly registered from the MCALT space to each subject space using ANTs. The gradient-echo images were used to calculate binary brain masks by thresholding magnitude images and then to reconstruct QSM images by using the STI suite (https://people.eecs.berkeley.edu/~chunlei.liu/software.html) (Li et al., 2015; Wu et al., 2012). QSM reconstruction process includes a Laplacian-based phase unwrapping (Schofield and Zhu, 2003), variable-kernel sophisticated harmonic artifact reduction for phase data method (Wu et al., 2012) for background field removal, and iterative least squares decomposition method (Li et al., 2015) for dipole inversion. The first-echo gradient-echo magnitude images were rigidly registered to the T1-weighted images, and then the obtained affine parameters were applied to brain masks and QSM images to apply the atlases for QSM images. Statistical Parametric Mapping (SPM12) was used for this rigid registration process. We performed a visual assessment and confirmed that the atlases were appropriately registered to the QSM images in all subjects. Tissue masks were created by multiplying the registered brain masks to the summed masks of gray and white matters. For voxel-based analysis, QSM images were spatially normalized into template space (MCALT space) using SPM12 after multiplying the tissue masks to exclude CSF signals and then smoothed by using a Gaussian kernel with 6-mm full-width at half maximum (FWHM). Tissue masks were also spatially normalized.

All flortaucipir PET scans were acquired on one of three PET/CT scanners, GE Discovery 690XT, GE Discovery MI, and Siemens Biograph64 Vision 600. For all PET/CT scans, a 20 min PET acquisition was performed 80 min after the injection with approximately 370MBq of [^{18}F] flortaucipir. The 20 min acquisition consisted of four 5-min dynamic scans. The PET images were reconstructed on-scanner using iterative algorithms (OSEM) with standard corrections and a 5 mm Gaussian post-reconstruction filter (Schwarz et al., 2022). The four-frame PET images were averaged after realignment and then rigidly registered to T1-weighted images to apply the brain atlases to the PET images. We performed a visual assessment and confirmed that the atlases were appropriately registered to the PET images in all subjects. The median values in the gray matter cerebellar crus were used to calculate standardized uptake value ratio (SUVR) images. For voxel-based analysis, SUVR images

were spatially normalized into template space using SPM12 and then smoothed using a Gaussian kernel with 6-mm FWHM.

The SUVRs and susceptibility values were obtained in seven subcortical ROIs in each subject space. The ROIs included the caudate, putamen, pallidum, subthalamic nucleus, substantia nigra, red nucleus, and cerebellar dentate. Note that the thalamus was not included because this region contains relatively many diamagnetic susceptibility sources such as myelin and calcium, as well as iron (Kumar et al., 2021). The midbrain was also not included because this region contains multiple sources of susceptibility; instead, the red nucleus and substantia nigra, which are part of the midbrain and have iron as a primary susceptibility source (Sun et al., 2015), were included. In each ROI, the mean values in the summed regions of gray and white matter masks were calculated on the left and right sides, respectively, and then both values were averaged. The MCALT atlas (Schwarz et al., 2017) was used for caudate, putamen, and pallidum ROIs; the Deep Brain Stimulation Intrinsic Template atlas (Ewert et al., 2018) was used for subthalamic nucleus, substantia nigra, and red nucleus ROIs; and an in-house developed atlas (Whitwell et al., 2017b) was used for the cerebellar dentate ROI. The positions of these subcortical ROIs are shown in Supplementary Fig. 1.

2.3. Statistical analysis

First, to assess patterns of abnormalities in these two modalities, SUVR and susceptibility were compared between PSP and control groups, respectively, by performing linear regression with age and sex as covariates (SUVR or susceptibility ~ group + age + sex) in the subcortical ROIs. The p-values obtained from the linear regression were adjusted using a false discovery rate (FDR) correction (Benjamini and Hochberg, 1995) to correct for the multiple comparisons of the seven ROIs.

The relationships between SUVR and susceptibility were then evaluated by using Spearman's partial correlation analysis adjusted for age and sex in the subcortical ROIs. This correlation analysis was performed separately for each group (PSP or control). The p-values from the correlation analysis were again adjusted by FDR correction (Benjamini and Hochberg, 1995). This regional correlation analysis was also performed after a two-compartment partial volume correction for PET images (Meltzer et al., 1999) and after using a whole-brain reference region for QSM images (Bilgic et al., 2023) for comparison. The analysis was also performed within each PSP clinical variant.

Voxel-based regression analysis was also performed for the whole brain in the template space to complement the ROI-based analysis. We used VoxelStats (Mathotaarachchi et al., 2016) which fits a linear regression in each voxel to evaluate the association between two modalities. Age and sex were adjusted for in this analysis (SUVR ~ susceptibility + age + sex). The analyzed regions were confined in the area where the averaged tissue masks of all subjects exceeded 0.95. Surviving regions were shown after applying the Random Field Theory (RFT)-based multiple comparison correction to the results (Mathotaarachchi et al., 2016).

Finally, the effects of susceptibility signals on flortaucipir uptake were examined by using the framework of mediation analysis. In this analysis, we hypothesized that the increased flortaucipir uptake in PSP was partially or fully explained by magnetic susceptibility based on the previous studies (Choi et al., 2018; Lowe et al., 2016). Therefore, the mediation model (Fig. 1) included flortaucipir SUVR as the dependent variable (outcome), magnetic susceptibility as the mediator, and diagnosis group (zero for control or one for PSP) as the independent variable. Based on this model, the coefficients for total effects (c_T, group effects on SUVR without mediator), direct effects (c_D, group effects on SUVR when susceptibility is considered), and indirect effects ($c_I = c_T - c_D$) were calculated using linear regression and mediation packages (Tingley et al., 2014) from R software (version 4.1.2). Age and sex were adjusted for in each linear regression. The 95 % confidence intervals for all coefficients were obtained by bootstrapping (1000 samples).

Demographic and clinical outcomes were compared between PSP and control groups by using a Fisher's exact test for categorical values and a Wilcoxon rank sum test for continuous values. Mediation analysis was performed by using R software, and all other statistical analyses were performed by using the MATLAB 2022a and its Statistics and Machine Learning Toolbox.

3. Results

The characteristics of the participants are shown in Table 1. There were no significant differences in sex between PSP and controls. However, years of education were lower ($p<0.01$), age was higher ($p<0.001$), and MoCA was lower ($p<0.001$) in PSP compared to controls.

Fig. 2 shows comparisons between PSP and controls in SUVR (Fig. 2a) and susceptibility (Fig. 2b). Both modalities showed similar patterns, with both showing greater signal in PSP ($p<0.05$) in the putamen, pallidum, subthalamic nucleus, red nucleus, and cerebellar dentate. However, in the caudate and substantia nigra, susceptibility was greater in PSP ($p<0.01$) than controls, while no difference was observed in SUVR.

Fig. 3 shows the relationships between magnetic susceptibility and flortaucipir uptake in the seven subcortical regions. Positive correlations were observed in PSP in the putamen, pallidum, subthalamic nucleus, red nucleus, and cerebellar dentate (all $p<0.05$). The pallidum was the only region that showed a correlation between magnetic susceptibility and flortaucipir uptake in controls. There were no significant correlations in both groups in the caudate and substantia nigra. The results were generally unchanged after partial volume correction for PET images (Supplementary Table 1) or after using the reference region for QSM images (Supplementary Table 2). No significant correlations were found between susceptibility and flortaucipir uptake within each PSP clinical variant (Supplementary Fig. 2).

Fig 4 shows the voxel-based relationships between flortaucipir and susceptibility. The results of the voxel-based analysis were consistent with the ROI-based analysis. As shown in Fig. 4a, positive associations were observed in the caudate, putamen, pallidum, thalamus,

subthalamic nucleus, and red nucleus in the PSP group. In addition, there were also positive associations in the bilateral frontal white matter and right fusiform region. As shown in Fig. 4b, there were positive associations in the caudate and pallidum in the control group. Negative associations were found only in two clusters around the lateral ventricle in PSP and one cluster in the left frontal lobe in controls (Supplementary Fig. 3).

Table 2 shows the results of the mediation analysis in the five subcortical regions (putamen, pallidum, subthalamic nucleus, red nucleus, and cerebellar dentate) where flortaucipir uptake was significantly greater in PSP than in controls. Direct effects were positive and significant in the putamen, pallidum, subthalamic nucleus, and red nucleus, but were not significant in the cerebellar dentate. Indirect effects were positive and significant in all five regions.

4. Discussion

In this study, we directly compared subcortical flortaucipir uptake and magnetic susceptibility in the same PSP cohort. Both flortaucipir and magnetic susceptibility had greater signal in PSP compared to controls in most subcortical regions (putamen, pallidum, subthalamic nucleus, red nucleus, and cerebellar dentate), while only magnetic susceptibility had greater signal in the caudate and substantia nigra. These results are generally consistent with previous PSP studies using flortaucipir PET (Cho et al., 2017; Passamonti et al., 2017; Whitwell et al., 2017b) or QSM (Ito et al., 2017; Sjostrom et al., 2017, 2019), respectively, with our study providing further validity with the same analysis techniques. Beyond validity, we directly compared the two modalities and show that they were positively correlated in most subcortical regions in PSP. Mediation analysis also revealed that greater flortaucipir uptake in PSP was partially or fully explained by magnetic susceptibility. Since QSM signals are associated with iron concentration in subcortical regions (Langkammer et al., 2012), these results suggest that some flortaucipir uptake is related to iron in PSP.

There are several possible explanations for the positive association between flortaucipir and susceptibility, including off-target binding to iron or iron-related proteins (e.g., ferritin) (Choi et al., 2018; Lowe et al., 2016) or possible coexistence of tau and iron (Pérez et al., 1998; Rao and Adlard, 2018), although this study cannot address the cause of this association. The control group had a positive association in the pallidum, and this result was consistent with one previous study (Choi et al., 2018). Given that cognitively and motorically normal subjects should not have iron-related tau deposition, this positive association in the pallidum may reflect direct or indirect off-target binding to iron, at least in controls. The PSP group had positive associations in more regions (five regions) than controls (one region), suggesting additional causes (e.g., coexistence of tau and iron) or simply reflecting wider inter-subject variabilities of susceptibility and flortaucipir uptake in PSP compared to the control group. The voxel-based analysis supported our regional analysis and additionally revealed a positive association in bilateral frontal white matter. Reduced integrity of the white matter in this region of the frontal lobe has been observed on diffusion tensor imaging in PSP (Whitwell et al., 2014). This suggests that the increased susceptibility may reflect a reduction in diamagnetic myelin due to white matter degeneration, and that this degeneration is related to tau deposition in PSP, while we should

be cautious about the interpretation of white matter susceptibility because of its tensorial nature (Li et al., 2012). Further histological and autoradiography studies may help better understanding of these positive associations.

The correlation coefficient between flortaucipir uptake and susceptibility was highest in the red nucleus. One of the possible explanations is that this strong correlation comes from the highest inter-subject variabilities of susceptibility and flortaucipir in this region, which may reflect the diverse clinical variants in our PSP cohort. Recent QSM studies suggest that the red nucleus susceptibility is the prominent biomarker to discriminate different clinical variants of PSP, with the highest susceptibility in PSP-RS and PSP-P (Satoh et al., 2023b). Our tau PET study also suggests that flortaucipir uptake in the red nucleus discriminates PSP-RS from other variants (Whitwell et al., 2020). Our results indicate that these two recent findings are related, and therefore, further investigation of the mechanisms underlying this strong correlation will be interesting.

The lack of association between flortaucipir uptake and susceptibility in the substantia nigra may be due to the contribution of neuromelanin. Neuromelanin is known to be abundant in the substantia nigra in normal subjects and reduced in PSP (Taniguchi et al., 2018), and studies have suggested off-target binding of flortaucipir to neuromelanin (Lowe et al., 2016; Marquie et al., 2017). Hence, the mixture of increased iron and decreased neuromelanin may have caused the loss of association between flortaucipir and magnetic susceptibility.

There was also no association in the caudate, presumably because this region was less affected in terms of iron and tau. Magnetic susceptibility was different between PSP and controls, but the absolute difference in median values and the inter-subject variability were relatively small in the caudate compared to other regions. Tau deposition was also assumed to be low, as there was no difference in flortaucipir uptake, whereas other regions may have stronger iron-related and iron-unrelated effects on flortaucipir uptake, as discussed below.

No significant correlations were found between susceptibility and flortaucipir uptake within each PSP clinical variant, but there was some variability in correlation coefficients across variants; PSP-Richardson syndrome had the strongest correlation in the cerebellar dentate, and PSP-Parkinsonism in the putamen, subthalamic nucleus, and red nucleus. These differences may reflect the pathological variability across different clinical variants (Dickson et al., 2010). Because the small number of patients in each group limited the firm conclusions in this subgroup analysis, future studies with a larger cohort will be needed to investigate relationships within different variants. Note that the MRPI in our PSP cohort was relatively low compared to literature values, reflecting the wide variability of clinical variants (Grijalva et al., 2022).

The framework of mediation analysis showed that all five regions had indirect effects, indicating that increased flortaucipir uptake in PSP were partially or fully explained by magnetic susceptibility. This result suggests that some flortaucipir uptake is related to iron. This analysis also showed that four regions (putamen, pallidum, subthalamic nucleus, and red nucleus) still had direct effects between diagnosis and flortaucipir uptake, which were not explained by magnetic susceptibility. The possible explanations are that this direct

effect is indicative of other off-target substances such as monoamine oxidase (Vermeiren et al., 2018), true 4R tau binding, or both. However, recent studies showed that monoamine oxidase did not significantly affect flortaucipir uptake (Wright et al., 2022). Additionally, these four regions are qualitatively consistent with the regions where the second-generation tau PET tracers (^{18}F-PM-PBB3 and ^{18}F-PI-2620) have increased signal in PSP (except that they also have increased signal in the substantia nigra) (Jin et al., 2023). The second-generation tracers have higher affinity for 4R tau, and some decreased off-target effects (Jin et al., 2023) and are therefore may more accurately reflect PSP tau distribution. Considering these studies, the direct effects in our study may represent true 4R tau uptake, although pathological validation will be required. In summary, the results of mediation analysis suggest that subcortical flortaucipir uptake may include iron-related (e.g., off-target binding to iron) and unrelated (e.g., iron-unrelated 4R tau) components.

The strength of this study was the novelty of directly comparing two advanced imaging techniques (flortaucipir PET and QSM) in the same and relatively large PSP cohort that included many different clinical variants of PSP, allowing correlation and mediation analyses to examine susceptibility effects on flortaucipir uptake. Our analyses also corrected for age, sex and accounted for multiple comparisons. This study also has several limitations. First, this study lacks autopsy confirmation. A careful diagnosis was made with detailed neurological tests and biomarkers, but there remains the possibility that other pathological diagnoses were not completely excluded. Second, age differed between the PSP and control groups, although correlation analysis was performed within each group and age effects were adjusted for all analyses. These limitations will be addressed in the future by including autopsy-confirmed PSP patients and age-matched controls. Third, there can be multiple sources of magnetic susceptibility in the brain, including potential confounders such as myelin and calcification, although the main sources will be iron in the subcortical regions (Langkammer et al., 2012). Fourth, the results may be affected by partial volume effects in PET images, especially in small structures such as the subthalamic nucleus and substantia nigra. The FWHM of the point spread function of our scanners has been estimated to be between 5 and 8 mm, which is comparable to the size of these small structures (Kolpakwar et al., 2021; Massey et al., 2017). Although we confirmed that the results were unchanged after partial volume correction, the results for these regions should be interpreted with caution. Finally, it should be noted that we simplified the mediation model that magnetic susceptibility induce flortaucipir signal changes (e.g., off-target binding (Choi et al., 2018; Lowe et al., 2016)) and to ignore possible opposite effects from flortaucipir to susceptibility (e.g., tau-induced iron accumulation (Lei et al., 2012)). Further longitudinal studies are needed to assess susceptibility effects more accurately on flortaucipir uptake.

5. Conclusion

We directly compared flortaucipir and susceptibility signals in the same PSP cohort. Both modalities had increased signal and positive correlations in many subcortical regions in PSP and we found evidence that flortaucipir uptake was partially or fully explained by susceptibility. These results suggest that some subcortical flortaucipir uptake may be associated with iron. These findings will contribute to our understanding of the mechanisms underlying flortaucipir tau PET signal in PSP, 4R tauopathies and other neurodegenerative

diseases, and should be considered in clinical treatment trials that utilize flortaucipir PET as an outcome measure.

Supplementary Material

Refer to Web version on PubMed Central for supplementary material.

Acknowledgments

This study is supported by NIH grants R01-NS89757, R01-DC12519, R01-DC14942 and RF1-NS112153. We would like to acknowledge AVID Radiopharmaceuticals for provision of AV-1451 precursor, chemistry production advice and oversight, and FDA regulatory cross-filing permission and documentation needed for this work. We also thank Dr. Christopher G. Schwarz for valuable discussion and support in PET imaging.

Data availability

The data that support the findings of this study are available from the corresponding author on reasonable request.

Abbreviations:

AD	Alzheimer's disease
PSP	progressive supranuclear palsy
4R	4 repeat
QSM	quantitative susceptibility mapping
NRG	Neurodegenerative Research Group
MoCA	Montreal Cognitive Assessment
MDS-UPDRS III	Movement Disorders Society sponsored revision of the Unified Parkinson's Disease Rating Scale part III
PSIS	PSP Saccadic Impairment Scale
MRPI	Magnetic Resonance Parkinsonism Index
MPRAGE	magnetization prepared rapid acquisition gradient echo
MCALT	Mayo Clinic Adult Lifespan Template
ROI	regions of interest
FWHM	full-width at half maximum
SUVR	standardized uptake value ratio
FDR	false discovery rate
RFT	random field theory

References

Benjamini Y, Hochberg Y, 1995. Controlling the false discovery rate: a practical and powerful approach to multiple testing. J. R. Stat. Soc. Ser. B Stat. Methodol. 57, 289–300.

Bilgic B, Costagli M, Chan K-S, Duyn J, Langkammer C, Lee J, Li X, Liu C, Marques JP, Milovic C, Robinson S, Schweser F, Shmueli K, Spincemaille P, Straub S, Zijl P.v., Wang Y, 2023. Recommended implementation of quantitative susceptibility mapping for clinical research in the brain: a consensus of the ISMRM ElectroMagnetic Tissue Properties Study Group. arXiv:2307.02306.

Carson N, Leach L, Murphy KJ, 2018. A re-examination of Montreal Cognitive Assessment (MoCA) cutoff scores. Int. J. Geriatr. Psychiatry 33, 379–388. [PubMed: 28731508]

Cho H, Choi JY, Hwang MS, Lee SH, Ryu YH, Lee MS, Lyoo CH, 2017. Subcortical (18)F-AV-1451 binding patterns in progressive supranuclear palsy. Mov. Disord. 32, 134–140. [PubMed: 27813160]

Choi JY, Cho H, Ahn SJ, Lee JH, Ryu YH, Lee MS, Lyoo CH, 2018. Off-target (18)F-AV-1451 binding in the basal ganglia correlates with age-related iron accumulation. J. Nucl. Med. 59, 117–120. [PubMed: 28775201]

Cogswell PM, Fan AP, 2023. Multimodal comparisons of QSM and PET in neurodegeneration and aging. Neuroimage 273, 120068. [PubMed: 37003447]

Cogswell PM, Wiste HJ, Senjem ML, Gunter JL, Weigand SD, Schwarz CG, Arani A, Therneau TM, Lowe VJ, Knopman DS, Botha H, Graff-Radford J, Jones DT, Kantarci K, Vemuri P, Boeve BF, Mielke MM, Petersen RC, Jack CR Jr., 2021. Associations of quantitative susceptibility mapping with Alzheimer's disease clinical and imaging markers. Neuroimage 224, 117433. [PubMed: 33035667]

Dickson DW, Ahmed Z, Algom AA, Tsuboi Y, Josephs KA, 2010. Neuropathology of variants of progressive supranuclear palsy. Curr. Opin. Neurol. 23, 394–400. [PubMed: 20610990]

Ewert S, Plettig P, Li N, Chakravarty MM, Collins DL, Herrington TM, Kuhn AA, Horn A, 2018. Toward defining deep brain stimulation targets in MNI space: a subcortical atlas based on multimodal MRI, histology and structural connectivity. Neuroimage 170, 271–282. [PubMed: 28536045]

Goetz CG, Tilley BC, Shaftman SR, Stebbins GT, Fahn S, Martinez-Martin P, Poewe W, Sampaio C, Stern MB, Dodel R, Dubois B, Holloway R, Jankovic J, Kulisevsky J, Lang AE, Lees A, Leurgans S, LeWitt PA, Nyenhuis D, Olanow CW, Rascol O, Schrag A, Teresi JA, van Hilten JJ, LaPelle N, Movement Disorder Society URTF, 2008. Movement Disorder Society-sponsored revision of the Unified Parkinson's Disease Rating Scale (MDS-UPDRS): scale presentation and clinimetric testing results. Mov. Disord. 23, 2129–2170. [PubMed: 19025984]

Golbe LI, Ohman-Strickland PA, 2007. A clinical rating scale for progressive supranuclear palsy. Brain 130, 1552–1565. [PubMed: 17405767]

Grijalva RM, Pham NTT, Huang Q, Martin PR, Ali F, Clark HM, Duffy JR, Utianski RL, Botha H, Machulda MM, Weigand SD, Ahlskog JE, Dickson DW, Josephs KA, Whitwell JL, 2022. Brainstem biomarkers of clinical variant and pathology in progressive supranuclear palsy. Mov. Disord. 37, 702–712. [PubMed: 34970796]

Grimm MJ, Respondek G, Stamelou M, Arzberger T, Ferguson L, Gelpi E, Giese A, Grossman M, Irwin DJ, Pantelyat A, Rajput A, Roeber S, van Swieten JC, Troakes C, Antonini A, Bhatia KP, Colosimo C, van Eimeren T, Kassubek J, Levin J, Meissner WG, Nilsson C, Oertel WH, Piot I, Poewe W, Wenning GK, Boxer A, Golbe LI, Josephs KA, Litvan I, Morris HR, Whitwell JL, Compta Y, Corvol JC, Lang AE, Rowe JB, Hoglinger GU, Movement Disorder Society-endorsed PSPSG, 2019. How to apply the movement disorder society criteria for diagnosis of progressive supranuclear palsy. Mov. Disord. 34, 1228–1232. [PubMed: 30884545]

Hauw JJ, Daniel SE, Dickson D, Horoupian DS, Jellinger K, Lantos PL, McKee A, Tabaton M, Litvan I, 1994. Preliminary NINDS neuropathologic criteria for Steele-Richardson-Olszewski syndrome (progressive supranuclear palsy). Neurology 44, 2015–2019. [PubMed: 7969952]

Hoehn MM, Yahr MD, 1967. Parkinsonism: onset, progression and mortality. Neurology 17, 427–442. [PubMed: 6067254]

Hoglinger GU, Respondek G, Stamelou M, Kurz C, Josephs KA, Lang AE, Mollenhauer B, Muller U, Nilsson C, Whitwell JL, Arzberger T, Englund E, Gelpi E, Giese A, Irwin DJ, Meissner WG, Pantelyat A, Rajput A, van Swieten JC, Troakes C, Antonini A, Bhatia KP, Bordelon Y, Compta Y, Corvol JC, Colosimo C, Dickson DW, Dodel R, Ferguson L, Grossman M, Kassubek J, Krismer F, Levin J, Lorenzl S, Morris HR, Nestor P, Oertel WH, Poewe W, Rabinovici G, Rowe JB, Schellenberg GD, Seppi K, van Eimeren T, Wenning GK, Boxer AL, Golbe LI, Litvan I, Movement Disorder Society-endorsed PSPSG, 2017. Clinical diagnosis of progressive supranuclear palsy: the movement disorder society criteria. Mov. Disord. 32, 853–864. [PubMed: 28467028]

Ito K, Ohtsuka C, Yoshioka K, Kameda H, Yokosawa S, Sato R, Terayama Y, Sasaki M, 2017. Differential diagnosis of parkinsonism by a combined use of diffusion kurtosis imaging and quantitative susceptibility mapping. Neuroradiology 59, 759–769. [PubMed: 28689259]

Jin J, Su D, Zhang J, Li X, Feng T, 2023. Tau PET imaging in progressive supranuclear palsy: a systematic review and meta-analysis. J. Neurol. 270, 2451–2467. [PubMed: 36633672]

Josephs KA, Katsuse O, Beccano-Kelly DA, Lin WL, Uitti RJ, Fujino Y, Boeve BF, Hutton ML, Baker MC, Dickson DW, 2006. Atypical progressive supranuclear palsy with corticospinal tract degeneration. J. Neuropathol. Exp. Neurol. 65, 396–405. [PubMed: 16691120]

Kolpakwar S, Arora AJ, Pavan S, Kandadai RM, Alugolu R, Saradhi MV, Borgohain R, 2021. Volumetric analysis of subthalamic nucleus and red nucleus in patients of advanced Parkinson's disease using SWI sequences. Surg. Neurol. Int. 12, 377. [PubMed: 34513144]

Kovacs GG, Lukic MJ, Irwin DJ, Arzberger T, Respondek G, Lee EB, Coughlin D, Giese A, Grossman M, Kurz C, McMillan CT, Gelpi E, Compta Y, van Swieten JC, Laat LD, Troakes C, Al-Sarraj S, Robinson JL, Roeber S, Xie SX, Lee VM, Trojanowski JQ, Hoglinger GU, 2020. Distribution patterns of tau pathology in progressive supranuclear palsy. Acta Neuropathol. 140, 99–119. [PubMed: 32383020]

Kumar VJ, Scheffler K, Hagberg GE, Grodd W, 2021. Quantitative susceptibility mapping of the basal ganglia and thalamus at 9.4 Tesla. Front. Neuroanat. 15, 725731. [PubMed: 34602986]

Langkammer C, Schweser F, Krebs N, Deistung A, Goessler W, Scheurer E, Sommer K, Reishofer G, Yen K, Fazekas F, Ropele S, Reichenbach JR, 2012. Quantitative susceptibility mapping (QSM) as a means to measure brain iron? A post mortem validation study. Neuroimage 62, 1593–1599. [PubMed: 22634862]

Lei P, Ayton S, Finkelstein DI, Spoerri L, Ciccotosto GD, Wright DK, Wong BX, Adlard PA, Cherny RA, Lam LQ, Roberts BR, Volitakis I, Egan GF, McLean CA, Cappai R, Duce JA, Bush AI, 2012. Tau deficiency induces parkinsonism with dementia by impairing APP-mediated iron export. Nat. Med. 18, 291–295. [PubMed: 22286308]

Li W, Wang N, Yu F, Han H, Cao W, Romero R, Tantiwongkosi B, Duong TQ, Liu C, 2015. A method for estimating and removing streaking artifacts in quantitative susceptibility mapping. Neuroimage 108, 111–122. [PubMed: 25536496]

Li W, Wu B, Avram AV, Liu C, 2012. Magnetic susceptibility anisotropy of human brain in vivo and its molecular underpinnings. Neuroimage 59, 2088–2097. [PubMed: 22036681]

Lowe VJ, Curran G, Fang P, Liesinger AM, Josephs KA, Parisi JE, Kantarci K, Boeve BF, Pandey MK, Bruinsma T, Knopman DS, Jones DT, Petrucelli L, Cook CN, Graff-Radford NR, Dickson DW, Petersen RC, Jack CR Jr., Murray ME, 2016. An autoradiographic evaluation of AV-1451 Tau PET in dementia. Acta Neuropathol. Commun. 4, 58. [PubMed: 27296779]

Marquie M, Normandin MD, Meltzer AC, Siao Tick Chong M, Andrea NV, Anton-Fernandez A, Klunk WE, Mathis CA, Ikonomovic MD, Debnath M, Bien EA, Vanderburg CR, Costantino I, Makaretz S, DeVos SL, Oakley DH, Gomperts SN, Growdon JH, Domoto-Reilly K, Lucente D, Dickerson BC, Frosch MP, Hyman BT, Johnson KA, Gomez-Isla T, 2017. Pathological correlations of [F-18]-AV-1451 imaging in non-alzheimer tauopathies. Ann. Neurol. 81, 117–128. [PubMed: 27997036]

Massey LA, Miranda MA, Al-Helli O, Parkes HG, Thornton JS, So PW, White MJ, Mancini L, Strand C, Holton J, Lees AJ, Revesz T, Yousry TA, 2017. 9.4 T MR microscopy of the substantia nigra with pathological validation in controls and disease. Neuroimage Clin. 13, 154–163. [PubMed: 27981030]

Mathotaarachchi S, Wang S, Shin M, Pascoal TA, Benedet AL, Kang MS, Beaudry T, Fonov VS, Gauthier S, Labbe A, Rosa-Neto P, 2016. VoxelStats: a MATLAB package for multi-modal voxel-wise brain image analysis. Front. Neuroinform. 10, 20. [PubMed: 27378902]

Mattay VS, Fotenos AF, Ganley CJ, Marzella L, 2020. Brain tau imaging: food and drug administration approval of (18)F-flortaucipir injection. J. Nucl. Med. 61, 1411–1412. [PubMed: 32753388]

Meltzer CC, Kinahan PE, Greer PJ, Nichols TE, Comtat C, Cantwell MN, Lin MP, Price JC, 1999. Comparative evaluation of MR-based partial-volume correction schemes for PET. J. Nucl. Med. 40, 2053–2065. [PubMed: 10616886]

Nasreddine ZS, Phillips NA, Bédirian V, Charbonneau S, Whitehead V, Collin I, Cummings JL, Chertkow H, 2005. The Montreal Cognitive Assessment, MoCA: a brief screening tool for mild cognitive impairment. J. Am. Geriatr. Soc. 53, 695–699. [PubMed: 15817019]

Passamonti L, Vazquez Rodriguez P, Hong YT, Allinson KS, Williamson D, Borchert RJ, Sami S, Cope TE, Bevan-Jones WR, Jones PS, Arnold R, Surendranathan A, Mak E, Su L, Fryer TD, Aigbirhio FI, O'Brien JT, Rowe JB, 2017. 18F-AV-1451 positron emission tomography in Alzheimer's disease and progressive supranuclear palsy. Brain 140, 781–791. [PubMed: 28122879]

Pérez M, Valpuesta JM, De Garcini EM, Quintana C, Arrasate M, Carrascosa JL, Rábano A, De Yebenes JG, Avila J, 1998. Ferritin is associated with the aberrant tau filaments present in progressive supranuclear palsy. Am. J. Pathol. 152, 1531. [PubMed: 9626057]

Quattrone A, Nicoletti G, Messina D, Fera F, Condino F, Pugliese P, Lanza P, Barone P, Morgante L, Zappia M, Aguglia U, Gallo O, 2008. MR imaging index for differentiation of progressive supranuclear palsy from Parkinson disease and the Parkinson variant of multiple system atrophy. Radiology 246, 214–221. [PubMed: 17991785]

Rao SS, Adlard PA, 2018. Untangling tau and iron: exploring the interaction between iron and tau in neurodegeneration. Front. Mol. Neurosci. 11, 276. [PubMed: 30174587]

Satoh R, Arani A, Senjem ML, Duffy JR, Clark HM, Utianski RL, Botha H, Machulda MM, Jack CR, Whitwell JL, Josephs KA, 2023a. Spatial patterns of elevated magnetic susceptibility in progressive apraxia of speech. Neuroimage Clin. 38, 103394. [PubMed: 37003130]

Satoh R, Weigand SD, Pham NTT, Ali F, Arani A, Senjem ML, Jack CR Jr., Whitwell JL, Josephs KA, 2023b. Magnetic susceptibility in progressive supranuclear palsy variants, Parkinson's disease, and corticobasal syndrome. Mov. Disord. 38, 2282–2290. [PubMed: 37772771]

Schofield MA, Zhu Y, 2003. Fast phase unwrapping algorithm for interferometric applications. Opt. Lett. 28, 1194–1196. [PubMed: 12885018]

Schwarz CG, Gunter JL, Ward CP, Vemuri P, Senjem ML, Wiste HJ, Petersen RC, Knopman DS, Jack CR Jr., 2017. The Mayo Clinic Adult Lifespan Template: better quantification across the lifespan. Alzheimers Dement. 13, 792. [PubMed: 28174070]

Schwarz CG, Kremers WK, Lowe VJ, Savvides M, Gunter JL, Senjem ML, Vemuri P, Kantarci K, Knopman DS, Petersen RC, Jack CR Jr., Alzheimer's Disease Neuroimaging Initiative, 2022. Face recognition from research brain PET: an unexpected PET problem. Neuroimage 258, 119357. [PubMed: 35660089]

Singh NA, Arani A, Graff-Radford J, Senjem ML, Martin PR, Machulda MM, Schwarz CG, Shu Y, Cogswell PM, Knopman DS, Petersen RC, Lowe VJ, Jack CR Jr., Josephs KA, Whitwell JL, 2022. Distinct brain iron profiles associated with logopenic progressive aphasia and posterior cortical atrophy. Neuroimage Clin. 36, 103161. [PubMed: 36029670]

Sjostrom H, Granberg T, Westman E, Svenningsson P, 2017. Quantitative susceptibility mapping differentiates between parkinsonian disorders. Parkinsonism Relat. Disord. 44, 51–57. [PubMed: 28886909]

Sjostrom H, Surova Y, Nilsson M, Granberg T, Westman E, van Westen D, Svenningsson P, Hansson O, 2019. Mapping of apparent susceptibility yields promising diagnostic separation of progressive supranuclear palsy from other causes of parkinsonism. Sci. Rep. 9, 6079. [PubMed: 30988382]

Smith R, Schain M, Nilsson C, Strandberg O, Olsson T, Hagerstrom D, Jogi J, Borroni E, Scholl M, Honer M, Hansson O, 2017. Increased basal ganglia binding of (18) F-AV-1451 in patients with progressive supranuclear palsy. Mov. Disord. 32, 108–114. [PubMed: 27709757]

Sun H, Walsh AJ, Lebel RM, Blevins G, Catz I, Lu JQ, Johnson ES, Emery DJ, Warren KG, Wilman AH, 2015. Validation of quantitative susceptibility mapping with Perls' iron staining for subcortical gray matter. Neuroimage 105, 486–492. [PubMed: 25462797]

Taniguchi D, Hatano T, Kamagata K, Okuzumi A, Oji Y, Mori A, Hori M, Aoki S, Hattori N, 2018. Neuromelanin imaging and midbrain volumetry in progressive supranuclear palsy and Parkinson's disease. Mov. Disord. 33, 1488–1492. [PubMed: 29756366]

Tingley D, Yamamoto T, Hirose K, Keele L, Imai K, 2014. Mediation: R package for causal mediation analysis. J. Stat. Softw. 59.

Vermeiren C, Motte P, Viot D, Mairet-Coello G, Courade JP, Citron M, Mercier J, Hannestad J, Gillard M, 2018. The tau positron-emission tomography tracer AV-1451 binds with similar affinities to tau fibrils and monoamine oxidases. Mov. Disord. 33, 273–281. [PubMed: 29278274]

Wang Y, Liu T, 2015. Quantitative susceptibility mapping (QSM): decoding MRI data for a tissue magnetic biomarker. Magn. Reson. Med. 73, 82–101. [PubMed: 25044035]

Whitwell JL, Hoglinger GU, Antonini A, Bordelon Y, Boxer AL, Colosimo C, van Eimeren T, Golbe LI, Kassubek J, Kurz C, Litvan I, Pantelyat A, Rabinovici G, Respondek G, Rominger A, Rowe JB, Stamelou M, Josephs KA, Movement Disorder Society-endorsed PSPSG, 2017a. Radiological biomarkers for diagnosis in PSP: where are we and where do we need to be? Mov. Disord. 32, 955–971. [PubMed: 28500751]

Whitwell JL, Lowe VJ, Tosakulwong N, Weigand SD, Senjem ML, Schwarz CG, Spychalla AJ, Petersen RC, Jack CR Jr., Josephs KA, 2017b. [(18) F]AV-1451 tau positron emission tomography in progressive supranuclear palsy. Mov. Disord. 32, 124–133. [PubMed: 27787958]

Whitwell JL, Master AV, Avula R, Kantarci K, Eggers SD, Edmonson HA, Jack CR Jr., Josephs KA, 2011. Clinical correlates of white matter tract degeneration in progressive supranuclear palsy. Arch. Neurol. 68, 753–760. [PubMed: 21670399]

Whitwell JL, Schwarz CG, Reid RI, Kantarci K, Jack CR Jr., Josephs KA, 2014. Diffusion tensor imaging comparison of progressive supranuclear palsy and corticobasal syndromes. Parkinsonism Relat. Disord. 20, 493–498. [PubMed: 24656943]

Whitwell JL, Tosakulwong N, Botha H, Ali F, Clark HM, Duffy JR, Utianski RL, Stevens CA, Weigand SD, Schwarz CG, Senjem ML, Jack CR, Lowe VJ, Ahlskog JE, Dickson DW, Josephs KA, 2020. Brain volume and flortaucipir analysis of progressive supranuclear palsy clinical variants. Neuroimage Clin. 25, 102152. [PubMed: 31935638]

Williams DR, Holton JL, Strand C, Pittman A, de Silva R, Lees AJ, Revesz T, 2007. Pathological tau burden and distribution distinguishes progressive supranuclear palsy-parkinsonism from Richardson's syndrome. Brain 130, 1566–1576. [PubMed: 17525140]

Wright JP, Goodman JR, Lin YG, Lieberman BP, Clemens J, Gomez LF, Liang Q, Hoye AT, Pontecorvo MJ, Conway KA, 2022. Monoamine oxidase binding not expected to significantly affect [(18)F]flortaucipir PET interpretation. Eur. J. Nucl. Med. Mol. Imaging 49, 3797–3808. [PubMed: 35596745]

Wu B, Li W, Guidon A, Liu C, 2012. Whole brain susceptibility mapping using compressed sensing. Magn. Reson. Med. 67, 137–147. [PubMed: 21671269]

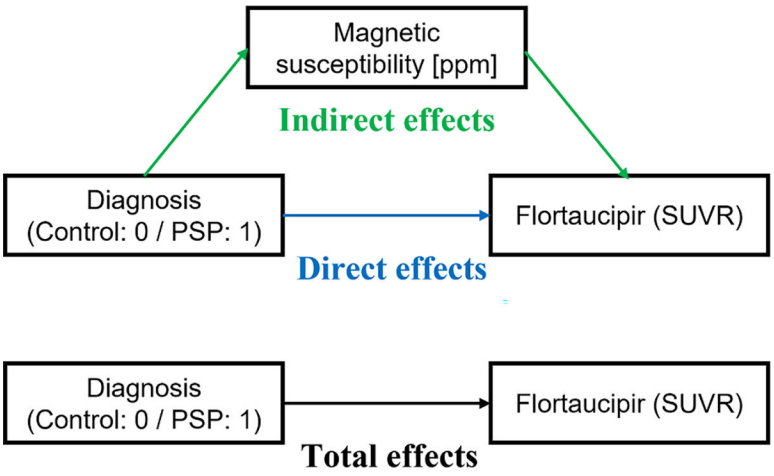

Fig. 1.

Schematic of the mediation analysis model. This model assumes that increased flortaucipir uptake in PSP is partially or fully explained by magnetic susceptibility (e.g., iron-related flortaucipir uptake).

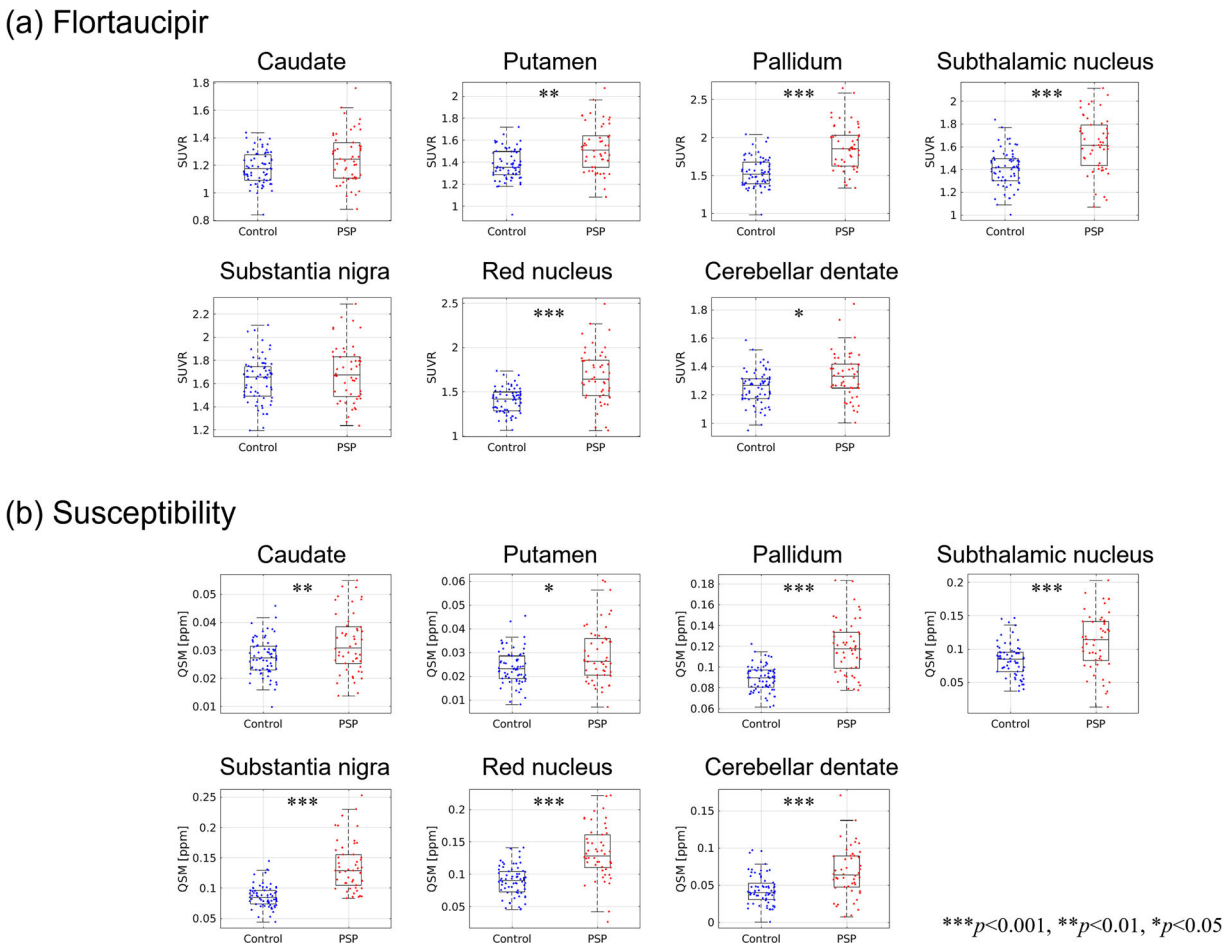

Fig. 2.

Boxplots of flortaucipir SUVR and susceptibility in the seven subcortical regions. Linear regression with age and sex as covariates and FDR adjustment for multiple comparisons of seven regions were used to calculate p-values.

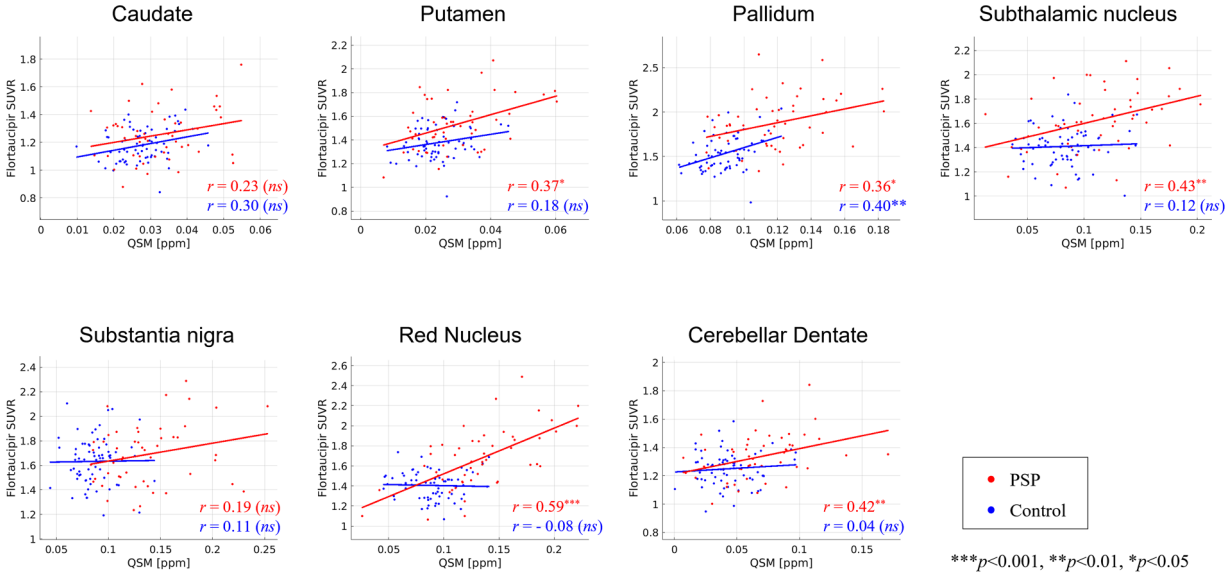

Fig. 3.

Relationship between flortaucipir uptake and susceptibility in subcortical regions. Red and blue dots show the scatter plots of these two signals in the PSP and control cohorts, respectively, and solid lines show linear regression lines. Spearman's partial correlation coefficients (r) adjusted for age and sex are shown in each panel. Their p-values were adjusted for multiple comparisons of seven regions. Abbreviation: ns = nonsignificant.

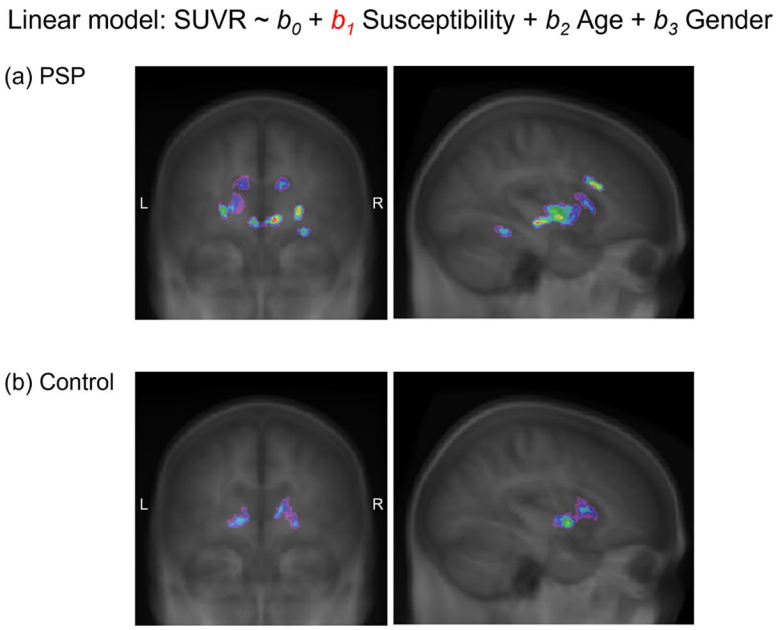

Fig. 4.

Voxel-level regional correlations between flortaucipir and susceptibility across the whole brain. Linear regression was calculated for each voxel with the age and sex as covariates. Results are presented using the $p<0.001$ threshold and RFT-based multiple comparison correction. Linear regression and these glass brain visualizations were performed using VoxelStats.

Table 1

Demographics and clinical findings for control and PSP groups. The parentheses indicate interquartile ranges.

	Control (*n* = 67)	**PSP (*n* = 50)**	***P***
Female, n (%)	46 (69 %)	26 (52 %)	0.09
Education, y	16 (16, 18)	14 (12, 18)	<0.01
Age, y	66.2 (58.1, 70.1)	71.0 (65.9, 77.2)	<0.001
Onset age, y		65.9 (60.7, 72.8)	
Disease duration, y		4.0 (2.6, 6.7)	
MoCA (/30)	27 (26, 28)	25 (19, 26)	<0.001
MDS-UPDRS III (/132)		39 (30, 56)	
PSP rating scale (/100)		36 (27, 43)	
PSIS (/5)		2 (1, 3)	
MRPI		14 (10, 19)	

Table 2

The results of mediation analysis. Each row contains total effects, direct effects, indirect effects, and proportion mediated. The parentheses indicate 95 % confidence interval for each variable.

	Total effect	Direct effect	Indirect effect	Prop. mediated
Putamen	**0.099** ** (0.025, 0.17)	**0.072** * (0.009, 0.13)	**0.027** * (0.002, 0.06)	27 %
Pallidum	**0.291** *** (0.192, 0.39)	**0.138** ** (0.032, 0.25)	**0.153** *** (0.078, 0.23)	53 %
Subthalamic nucleus	**0.207** *** (0.122, 0.29)	**0.152** *** (0.067, 0.24)	**0.054** ** (0.018, 0.10)	26 %
Red nucleus	**0.254** *** (0.160, 0.34)	**0.121** ** (0.043, 0.21)	**0.133** *** (0.068, 0.20)	52 %
Cerebellar dentate	**0.064** * (0.004, 0.12)	0.027 (−0.030, 0.08)	**0.038** ** (0.014, 0.07)	59 %

*** $p<0.001$.

** $p<0.01$.

* $p<0.05$.